

Robust two-qubit gates in a linear ion crystal using a frequency-modulated driving force

Pak Hong Leung,^{1,*} Kevin A. Landsman,² Caroline Figgatt,²
Norbert M. Linke,² Christopher Monroe,² and Kenneth R. Brown^{1,3}

¹*School of Physics, Georgia Institute of Technology, Atlanta, Georgia 30332, USA*

²*Joint Quantum Institute and Joint Center for Quantum Information and Computer Science, University of Maryland, College Park, MD 20742, USA*

³*Schools of Chemistry and Biochemistry and Computational Science and Engineering, Georgia Institute of Technology, Atlanta, Georgia 30332, USA*

(Dated: July 17, 2022)

In an ion trap quantum computer, collective motional modes are used to entangle two or more qubits in order to execute multi-qubit logical gates. Any residual entanglement between the internal and motional states of the ions will result in decoherence errors, especially when there are many spectator ions in the crystal. We propose using a frequency-modulated (FM) driving force to minimize such errors and implement it experimentally. In simulation, we obtained an optimized FM gate that can suppress decoherence to less than 10^{-4} and is robust against a frequency drift of more than ± 1 kHz. The two-qubit gate was tested in a five-qubit trapped ion crystal, with 98.3(4)% fidelity for a Mølmer-Sørensen entangling gate and 98.6(7)% for a controlled-not (CNOT) gate. We also show an optimized FM two-qubit gate for 17 ions, proving the scalability of our method.

Ion traps are a leading candidate for the realization of a quantum computer. Magnetically insensitive qubit energy splittings, long coherence times, and high-fidelity state initialization and detection [1, 2] prove to be significant advantages for trapped ion qubits. Individual qubit addressing and single-qubit gates with error rates on the order of 10^{-5} per gate have been achieved [1, 3–5]. Multiple qubits can be entangled through state-dependent forces driven by external fields [6–9], and for exactly two ions, entangling gate fidelities routinely exceed 99% and in some cases 99.9%. [10–14].

With increasing ion number, the motional modes bunch in frequency, which means exciting only a single motional mode becomes prohibitively slow. Alternatively, the state-dependent driving forces can couple to all modes of motion. A number of schemes have been proposed for disentangling the internal qubit states from the motional states of all modes by introducing variations to the driving force during the gate. One way to achieve this goal is amplitude modulation (AM) of the driving field [15, 16]. Several experiments have adopted this method and have achieved a 2 to 5% error [17–19]. Phase modulation has also been proposed for the same purpose, but the number of pulses in the sequence increases exponentially with the number of ions [20]. Both schemes require large, instantaneous changes to the electric field surrounding the ions, which may be hard to realize physically and can lead to gate errors not accounted for in experiments.

We propose a novel decoupling method through continuous frequency modulation (FM) which involves only

small and smooth oscillations of the detuning of the applied field (Fig. 1). We describe an optimized FM two-qubit gate that minimizes state-dependent displacement while maintaining robustness against frequency drifts up to the first order. Simulated and experimental results for a 5-ion trap are presented. Further theoretical justification is provided in the supplementary section.

To execute the Mølmer-Sørensen gate, we apply a state-dependent driving force to a pair of ions to entangle them through the collective motion of all the ions in the trap. As a result, every motional mode experiences a coherent displacement that is characterized by the displacement operator: $\hat{D}(\hat{\alpha}_k) = \exp(\hat{\alpha}_k a_k^\dagger - \hat{\alpha}_k^\dagger a_k)$. The state-dependent displacement is:

$$\hat{\alpha}_k(t) = \frac{\Omega}{2}(\eta_{i,k}\sigma_\phi^i + \eta_{j,k}\sigma_\phi^j) \int_0^t e^{i\theta_k(t')} dt' \quad (1)$$

where Ω is the carrier coupling strength, $\eta_{i,k}$ and $\eta_{j,k}$ are the Lamb-Dicke parameters of ions i and j with respect to mode k , σ_ϕ^i and σ_ϕ^j are bit-flip Pauli operators for the addressed ions, and $\theta_k(t) = \int_0^t \delta_k(t') dt'$ is the phase of the driving force relative to mode k . We define the associated scalar quantity:

$$\alpha_k(t) = \tilde{\eta}\tilde{\Omega} \int_0^t e^{i\theta_k(t')} dt' \quad (2)$$

where $\tilde{\eta}$ and $\tilde{\Omega}$ are the characteristic sizes of the Lamb-Dicke parameter and laser intensity required to entangle an ion pair. We may visualize the trajectory of $\alpha_k(t)$ by plotting it in the complex plane. This is the phase space trajectory (PST) of the motional mode k (Fig. 2). For a total gate time τ , $\alpha_k(0) = 0$ and $\alpha_k(\tau)$ are the beginning and end points of the PST.

* pleung6@gatech.edu

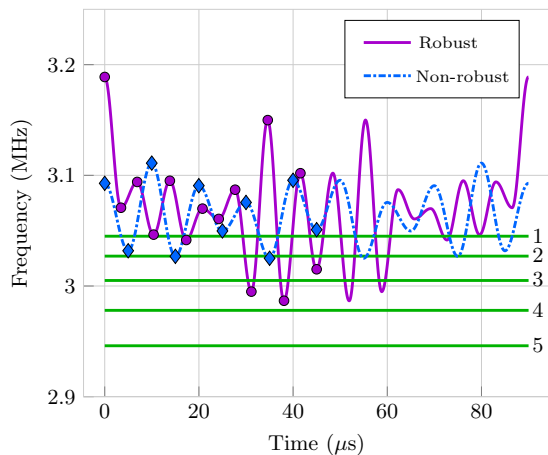


FIG. 1. Robust (violet, solid) and non-robust (blue, dash-dotted) FM pulses for 2-qubit gate optimized for 5 ions, both with a gate time of $90 \mu\text{s}$. Green lines are experimental sideband frequencies, labeled 1 to 5, the first one being the common mode frequency. The pulses are designed to be symmetric in time. The dots and diamonds represent the control parameters allowed to vary in our optimization algorithm.

Due to the state-dependent nature of $\hat{\alpha}_k(t)$, different eigenstates of the spin operator follow different paths in the PSTs. The resulting entanglement between spin and motion will therefore lead to decoherence unless $\alpha_k(\tau)$ is zero. To evaluate the decoherence error due to this residual internal-motional coupling, we represent the state as a density matrix, trace out the motional state space, and calculate its inner product with the target state, the Bell state. For example, suppose the starting state is $|\downarrow\downarrow\rangle$, and the ions are all cooled to the ground state. The gate fidelity is affected by residual entanglement with the common motional mode according to:

$$F = \frac{1}{8} (3 + 4e^{-|\alpha|^2/2} + e^{-2|\alpha|^2}) \approx 1 - \frac{|\alpha|^2}{2} \quad (3)$$

To consider contributions from other modes, which have different Lamb-Dicke parameters, we use the following estimate for the total error:

$$\varepsilon = \sum_{k=1}^N |\alpha_k(\tau)|^2 \quad (4)$$

Therefore, minimizing $|\alpha_k|$ is the most straightforward optimization criterion. However, in actual experiments the motional sidebands tend to drift slowly over time ($\delta_k \rightarrow \delta_k + \delta_1$ and $\delta_1 \ll 1/\tau$). We present a condition that makes the gate robust against δ_1 to first order. By expanding $e^{i\delta_1 t} \approx 1 + i\delta_1 t$ and using integration by parts (see supplementary section), the robustness condition is:

$$\alpha_{k,avg} \sim \int_0^\tau \int_0^t e^{i\theta_k(t')} dt' dt = 0 \quad (5)$$

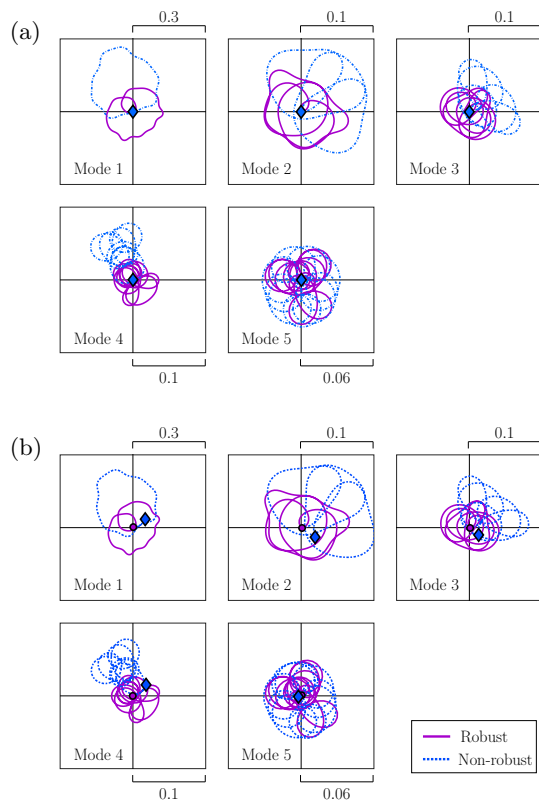


FIG. 2. simulated PSTs with: (a) no frequency error and (b) -1 kHz sideband drift, using the FM pulses shown in Fig. 1. The end points for the robust pulse (circles) return to the starting point under the drift, whereas those for non-robust (diamonds) fail to do so. The horizontal and vertical axes represent the quadratures $x_k \sim a_k^\dagger + a_k$ and $p_k \sim i(a_k^\dagger - a_k)$ respectively.

The double integral is proportional to the time-averaged position of $\alpha_{k,avg}(t)$ during the gate. It turns out that if we only consider symmetric pulses ($\delta_k(\tau-t) = \delta_k(t)$), $\alpha_{k,avg} = 0$ also guarantees that $\alpha_k = 0$. This simplifies the optimization process for robust pulses.

By observing the formula for the displacement $\alpha_k(t)$, we note that the phase space trajectory moves with constant speed but varying angular rate $\delta_k(t)$, which is proportional to the curvature. In this paper, we minimize $\alpha_k(\tau)$ and $\alpha_{k,avg}(\tau)$ by introducing variations in $\delta_k(t)$, or modulating the driving frequency during the gate, which changes the curvature of the trajectory for every motional mode continuously (see Fig. 2). The detunings for different modes are correlated, however, since increasing (decreasing) the driving frequency increases (decreases) the detunings for all modes. Thus we have a multivariate optimization problem.

The vertices (local maxima and minima) of the frequency pattern are chosen as the optimization parameters (purple dots and blue diamonds in Fig. 1). Sinusoidal functions are then used to connect these vertices, creating a smooth and continuous frequency profile. The

function to be minimized is $|\alpha_{k,avg}|^2$ for robust pulses and $|\alpha_k|^2$ for non-robust. We evaluate the gradient for these functions with respect to the parameters, and perform minimization using quasi-Newton methods. In our simulation, the BFGS (Broyden-Fletcher-Goldfarb-Shanno)

algorithm from the SciPy package was used. The optimized solution vector is then used to find the final trajectories and decoherence error for with and without a frequency drift.

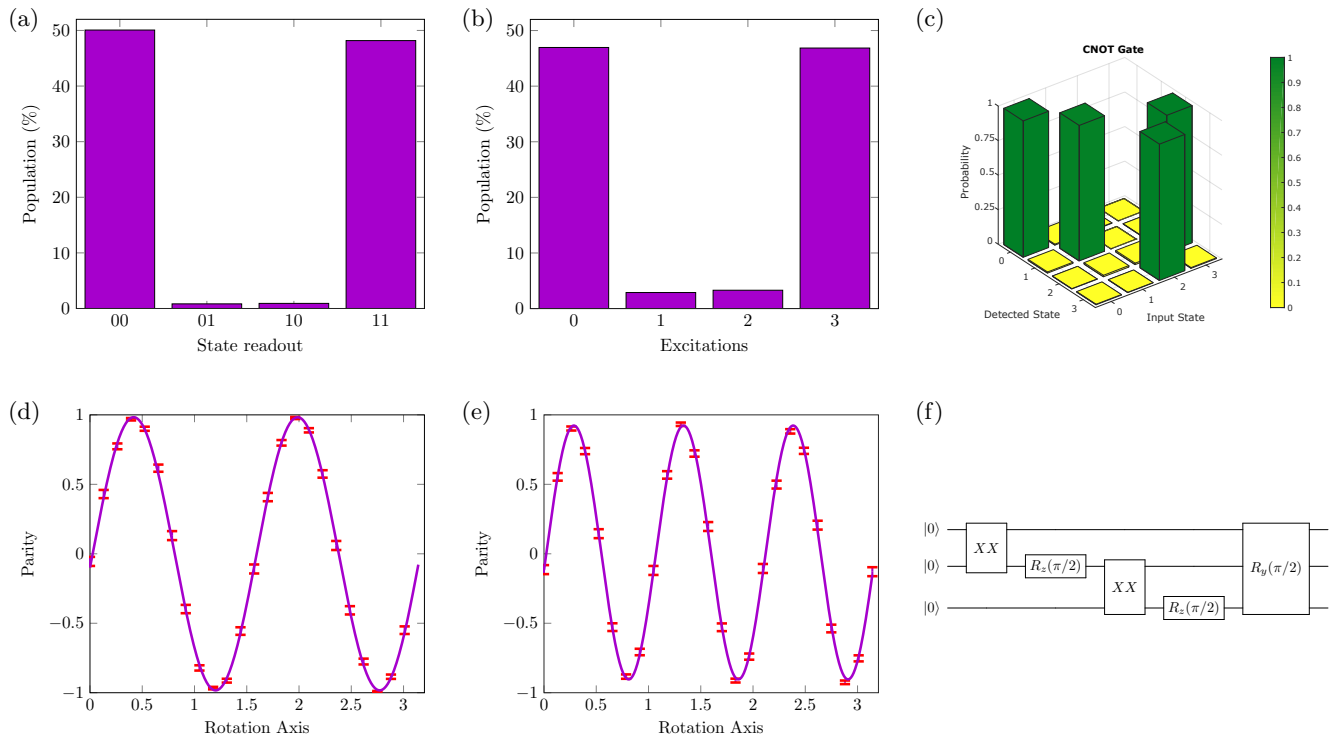


FIG. 3. (a) State population and (b) parity scan of the two qubits after the FM gate, indicating a fidelity of 98.3(4)%. (c) The probability of each output state for any input state after the CNOT gate, with fidelity 98.6(7)%. (d) Combined population for any number of excitation and (e) parity scan of the output 3-qubit GHZ state. (f) The circuit used to generate the 3-qubit GHZ state.

Finally, we estimate the power required to entangle the qubits by computing the areas enclosed by the PSTs and the sum of those areas weighted by the respective Lamb-Dicke parameters obtained from simulation (see supplementary section). Note that if the power is too high to implement experimentally, we may simply repeat the pulse R times to reduce the amount of power used by \sqrt{R} . This will lengthen the gate time without greatly reducing the robustness of the pulse.

In our experiment, 5 $^{171}\text{Yb}^+$ ions are held in an rf Paul trap with a radial trap frequency of 3.045 MHz and an average ion separation of about 5 μm . Our qubit is defined by the ground hyperfine states $^2\text{S}_{1/2}, |F=0\rangle$ and $^2\text{S}_{1/2}, |F=1\rangle$ with an energy splitting of $2\pi \times 12.642821$ GHz. Initially, all ions are cooled to close to the motional ground state (≈ 0.1 phonons) and then optically pumped to the $|0\rangle$ state. Quantum gates are implemented using a beatnote generated by counter-propagating Raman laser beams that are capable of addressing any individual qubit

[19].

The transverse motional sidebands are measured and used to find the optimal FM pulses for the 2-qubit gate. With a fixed gate time of 90 μs , the optimized robust pulse consists of 13 oscillations (Fig. 1), whereas the non-robust version has only 9. PSTs are plotted for no frequency error and for a 1 kHz frequency drift for both robust and non-robust pulses in Fig. 2. Under the drift, the end points of the robust trajectory (circles) stick to the origin, whereas those of the non-robust (diamonds) deviate from the starting point, causing a decoherence error of about 0.5%. This demonstrates the importance of the robustness feature.

We experimentally test both the robust and non-robust version of the gate on our 5-ion computer, and use it to entangle two neighboring ions on one edge of the ion chain. The output population and the parity are measured and shown in Figs. 3(a) and (b), giving a SPAM-corrected fidelity of 98.3(4)%. To perform a CNOT gate,

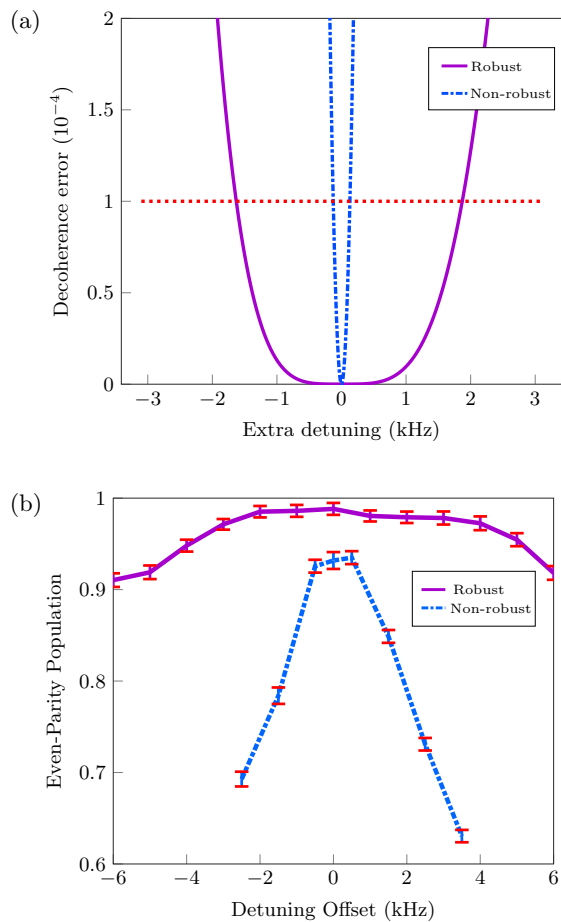


FIG. 4. (a) Simulated decoherence error and (b) Experimental even-parity populations of the two qubits after the gate for a range of detuning offsets. The robust gate has a significantly better performance than non-robust in both theory and experiment

we perform additional single-qubit rotations before and after the two-qubit entangling gate, and find a fidelity of 98.6(7)% (Fig. 3(c)). These results are very similar to the fidelity achieved with optimized AM gates. We also successfully create a 3-qubit GHZ state with a fidelity of 92.6(3)% (Figs. 3(d)-(f)).

We perform the gate by applying the optimized pulse twice sequentially ($R = 2$) with a laser intensity corresponding to a carrier Rabi frequency of $2\pi \times 600$ kHz. The combined gate time is therefore $180 \mu s$. But according to simulation results, the power required Ω for maximum entanglement for $R = 2$ ranges from $2\pi \times 151$ kHz for neighboring qubits to $2\pi \times 246$ kHz for qubits on opposite ends of the ion chain. The higher-than-expected power requirement is most likely due to an overestimate of the Lamb-Dicke parameters in our simulation (see supplementary section for formula). The high power used will also worsen other error sources such as unwanted carrier coupling and crosstalk with other qubits.

The theoretically estimated decoherence error is plot-

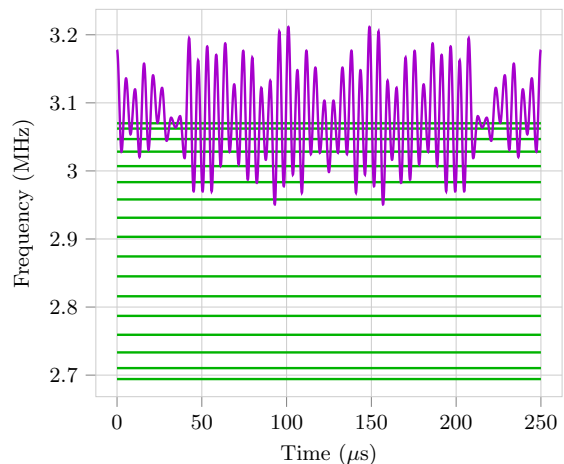


FIG. 5. Robust FM pulse for 2-qubit gate for 17 ions, with 47 oscillations. The motional mode frequencies (green lines) are obtained from the simulation of an anharmonic trap.

ted as a function of frequency drift in Fig. 4(a), highlighting the robustness of the gate. The error is less than 10^{-4} for a frequency errors up to ± 1.5 kHz for the robust pulse, but less than ± 0.1 kHz for non-robust. The non-robust pulse has a quadratic dependence on the drift, whereas the robust version has a quartic dependence. This is expected, since error is proportional to displacement squared, and the first-order dependence of the displacement on drift is cancelled out in the robust μ case.

To determine the impact of sideband drifts, we experimentally run the two gates over a range of symmetric detunings Fig. 4(b). The robust version has fidelity (even-parity population) higher than 90% for frequency offsets up to ± 5 kHz, whereas the non-robust gate has significantly lower fidelity and tolerance towards frequency errors (within ± 1 kHz), confirming the power of the robust method to improve fidelity by canceling frequency drifts.

We have run a similar optimization for 17 $^{171}\text{Yb}^+$ ions, motivated by the 17-qubit surface code proposed for quantum error correction [21–23], and in order to generalize our method for more qubits. The sideband frequencies for 17 ions are calculated from a simulated anharmonic ion trap with an average ion separation of about $3.5 \mu m$. Such high ion density may be challenging to realize with current technology, but that does not pose a fundamental physical limit and may be overcome with future experimental improvements.

The robust FM pulse obtained consists of 47 oscillations within a gate time of $250 \mu s$ (Fig. 5). The decoherence error exceeds 10^{-4} for a frequency drift of 500 Hz. Apparently, the gate is more sensitive to frequency errors due to an increased number of motional modes and a longer gate time.

As we increase the distance between the ions be entangled, the power required (Ω) for the two-qubit gate

ranges from $2\pi \times 115$ kHz to $2\pi \times 249$ kHz. This is an encouraging result. Previous theories indicate that the gate time and power required for entangling gates increase very quickly with the distance between the ions. The FM optimization method presented here overcomes this difficulty. We also speculate that the slowdown of our two-qubit gate may be alleviated by leveraging all motional modes of the ion crystal.

We have shown that we can perform high-fidelity two-qubit gates using frequency modulation in a linear ion trap. In theory, the optimized robust FM pulse can suppress decoherence errors to below 10^{-4} for up to a ± 1.5 kHz frequency offset for 5 $^{171}\text{Yb}^+$ ions. The gate has been tested experimentally to entangle neighboring ions and has a fidelity of 98.6(7)%. We speculate that with technical improvements, we will attain the high fidelity previously achieved with 2-ion traps in the near future. [10, 14].

ACKNOWLEDGEMENTS

We would like to thank Todd Green, Luming Duan, and Gang Shu for useful discussions. This work was supported by the Office of the Director of National Intelligence - Intelligence Advanced Research Projects Activity through ARO contract W911NF-10-1-0231 and the ARO MURI on Modular Quantum Systems.

-
- [1] S. Olmschenk, K. C. Younge, D. L. Moehring, D. N. Matsukevich, P. Maunz, and C. Monroe, *Phys. Rev. A* **76**, 052314 (2007).
 - [2] R. Noek, G. Vrijsen, D. Gaultney, E. Mount, Taehyun, P. Maunz, and J. Kim, *Opt. Lett.* **38**, 4735 (2013).
 - [3] K. R. Brown, A. C. Wilson, Y. Colombe, C. Ospelkaus, A. M. Meier, E. Knill, D. Leibfried, and D. J. Wineland, *Phys. Rev. A* **84**, 030303 (2011).
 - [4] T. P. Harty, D. T. C. Allcock, C. J. Ballance, L. Guidoni, H. A. Janacek, N. M. Linke, D. N. Stacey, and D. M. Lucas, *Phys. Rev. Lett.* **113**, 220501 (2014).
 - [5] D. P. L. Aude Craik, N. M. Linke, M. A. Sepiol, T. P. Harty, J. F. Goodwin, C. J. Ballance, D. N. Stacey, A. M. Steane, D. M. Lucas, and D. T. C. Allcock, *Phys. Rev. A* **95**, 022337 (2017).
 - [6] K. Mølmer and A. Sørensen, *Phys. Rev. Lett.* **82**, 1835 (1999).
 - [7] A. Sørensen and K. Mølmer, *Phys. Rev. Lett.* **82**, 1971 (1999).
 - [8] G. Milburn, S. Schneider, and D. James, *Fortschritte der Physik* **48**, 801 (2000).
 - [9] E. Solano, R. L. de Matos Filho, and N. Zagury, *Phys. Rev. A* **59**, R2539 (1999).
 - [10] J. P. Gaebler, T. R. Tan, Y. Lin, Y. Wan, R. Bowler, A. C. Keith, S. Glancy, K. Coakley, E. Knill, D. Leibfried, and D. J. Wineland, *Phys. Rev. Lett.* **117**, 060505 (2016).

- [11] T. Monz, P. Schindler, J. T. Barreiro, M. Chwalla, D. Nigg, W. A. Coish, M. Harlander, W. Hänsel, M. Hennrich, and R. Blatt, *Phys. Rev. Lett.* **106**, 130506 (2011).
- [12] C. Ospelkaus, U. Warring, Y. Colombe, K. R. Brown, J. M. Amini, D. Leibfried, and D. J. Wineland, *Nature* **476**, 181 (2011).
- [13] T. P. Harty, M. A. Sepiol, D. T. C. Allcock, C. J. Ballance, J. E. Tarlton, and D. M. Lucas, *Phys. Rev. Lett.* **117**, 140501 (2016).
- [14] C. J. Ballance, T. P. Harty, N. M. Linke, M. A. Sepiol, and D. M. Lucas, *Phys. Rev. Lett.* **117**, 060504 (2016).
- [15] Shi-Liang Zhu, C. Monroe, and L.-M. Duan, *Europhys. Lett.* **73**, 485 (2006).
- [16] C. F. Roos, *New Journal of Physics* **10**, 013002 (2008).
- [17] K. Kim, M.-S. Chang, R. Islam, S. Korenblit, L.-M. Duan, and C. Monroe, *Phys. Rev. Lett.* **103**, 120502 (2009).
- [18] T. Choi, S. Debnath, T. A. Manning, C. Figgatt, Z.-X. Gong, L.-M. Duan, and C. Monroe, *Phys. Rev. Lett.* **112**, 190502 (2014).
- [19] S. Debnath, N. M. Linke, C. Figgatt, K. A. Landsman, K. Wright, and C. Monroe, *Nature* **536**, 63 (2016).
- [20] T. J. Green and M. J. Biercuk, *Phys. Rev. Lett.* **114**, 120502 (2015).
- [21] Y. Tomita and K. M. Svore, *Phys. Rev. A* **90**, 062320 (2014).
- [22] C. Horsman, A. G. Fowler, S. Devitt, and R. V. Meter, *New Journal of Physics* **14**, 123011 (2012).
- [23] A. M. Stephens, *Phys. Rev. A* **89**, 022321 (2014).

SUPPLEMENTARY SECTION

MØLMER-SØRENSEN GATE FOR VARYING DETUNING

This section reviews the physics of a standard Mølmer-Sørensen gate. Note that the most important generalization made in this paper is the time-dependence of detuning. The laser phase must be kept continuous, which should be more easily achieved in experiments than otherwise.

Suppose the driving field consists of two counter-propagating laser beams with the same intensity and opposite detunings, applied to any two ions in a linear N-ion crystal. We assume that the beams are perpendicular to the ion chain axis, so that only the transverse motional modes are excited. The ion-field interaction can be written as [6, 7]:

$$\hat{H}_{MS} = \frac{\Omega}{2} \sum_{k=1}^N S_{\phi,\gamma}^k a_k^\dagger e^{i\theta_k(t)} + S_{\phi,\gamma}^k a_k e^{-i\theta_k(t)} \quad (6)$$

where θ_k is the integrated phase of the detuning between the driving force and the k-th sideband, i.e. $\theta_k(t) = \int_0^t \delta_k(t') dt'$, and Ω is the effective Rabi frequency for the carrier transition using a particular laser intensity. S_{ϕ}^k equals $\eta_{i,k} \sigma_{\phi}^i + \eta_{j,k} e^{i\gamma} \sigma_{\phi}^j$, where $\sigma_{\phi} = \sigma_x \cos \phi + \sigma_y \sin \phi$ is a general spin flip operator about an

axis on the x-y plane, ϕ is half the relative phase between the two sidebands, and γ is the relative phase between the lasers applied to the two ions. $\eta_{j,k}$ is the Lamb-Dicke parameter for the j th ion and the k th motional mode, and is given by $\Delta k \sqrt{\frac{\hbar}{2m\omega_k}} u_{jk}$, where $\Delta k = 4\pi/\lambda$ is the wavenumber of the two counterpropagating Raman lasers ($\lambda = 355$ nm), and u_{jk} is the unitary matrix that maps ion coordinates to the resonant mode coordinates. Note that if the lasers are at an angle to the axis of motion, the parameter will be reduced by the cosine of that angle. The expression is valid if the Lamb-Dicke approximation holds ($\eta_{j,k} \sqrt{n + \frac{1}{2}} \ll 1$, $n = \sqrt{\langle a^\dagger a \rangle}$), and the direct carrier transition is small (Ω is much smaller than the detuning from the carrier transition).

The Hamiltonian consists of a sum of products of internal and motional operators, and thus represents a state-dependent force acting on the ion chain as a whole. To solve the time-dependent Schrödinger equation, we apply the Magnus expansion to compute the argument of the effective propagator [15, 16]:

$$|\psi(t)\rangle = \hat{D}(\{\hat{\alpha}_k\}) \hat{E}(\beta_{ij}) |\psi(0)\rangle \quad (7)$$

$$\hat{D}(\{\hat{\alpha}_k\}) = \exp\left(\sum_{k=1}^N (\hat{\alpha}_k a_k^\dagger - \hat{\alpha}_k^\dagger a_k)\right) \quad (8)$$

$$\text{where } \hat{\alpha}_k(t) = S_{\phi,\gamma}^k \frac{\Omega}{2} \int_0^t e^{i\theta_k(t')} dt'$$

$$\begin{aligned} \hat{E}(\beta_{ij}) &= \exp\left(-i\beta_{ij} \sigma_\phi^i \sigma_\phi^j\right) \\ &= \exp\left(-i\sigma_\phi^i \sigma_\phi^j \frac{\Omega^2}{2} \cos\gamma \sum_{k=1}^N \int_0^t \int_0^{t'} \eta_{i,k} \eta_{j,k} \right. \\ &\quad \left. \times \sin(\theta_k(t') - \theta_k(t'')) dt' dt''\right) \end{aligned} \quad (9)$$

The first term from the expansion is the direct time integral of the Hamiltonian and is proportional to $\hat{\alpha}_k a_k^\dagger - \hat{\alpha}_k^\dagger a_k$, which is the argument of the displacement operator and is related to quantum coherent states. The second term is the double time integral of the commutator of the Hamiltonian as functions of different time parameters, and is proportional to $\sigma_\phi^i \otimes \sigma_\phi^j$. Conveniently, higher-order terms vanish, and the two surviving terms commute, so we can express the final propagator as the product of two unitaries.

Consider the first operator $\hat{D}(\{\hat{\alpha}_k\})$, where the displacement $\hat{\alpha}_k$ is state-dependent and is proportional to the spin operator $S_{\phi,\gamma}^k$. If the internal state happens to be an eigenstate of $S_{\phi,\gamma}^k$, we may replace it with its eigenvalue, and \hat{D} simply displaces the motional state from one coherent state to another by α_k . We can plot the

2-D phase space trajectory (PST) to keep track of the complex displacement over time (Fig. 2). It is worth emphasizing that the quadrature axes in the PSTs do not represent the expected position or momentum of any particle like they do for a single quantum harmonic oscillator, since we are looking at the Hamiltonian in the interaction frame, and we are tracking down the collective instead of individual motion of the ions.

In general, the initial internal state is a superposition of the four eigenstates of $S_{\phi,\gamma}^k = \eta_{i,k} \sigma_\phi^i + \eta_{j,k} e^{i\gamma} \sigma_\phi^j$, and each eigenstate follows a different trajectory in the phase space according to its eigenvalue. In the PSTs in Fig. 2, we only track the trajectory of $|++\rangle_\phi$, where $|+\rangle_\phi$ is the positive eigenstate of σ_ϕ^i , in the case where the laser phase γ is zero. Since the trajectories for different eigenstates have different end points, there is a residual entanglement between the internal and motional state spaces, and will become a source of decoherence error since we only measure the internal qubit states. Thus, we need $\alpha_k(t) = 0$ in magnitude for all motional modes k in our optimization to guarantee that end points of the trajectories are sent back to their starting points.

The second operator \hat{E}_{ij} represents a rotation on the Bloch sphere spanned by $|\downarrow\downarrow\rangle$ and $|\uparrow\uparrow\rangle$. For maximal entanglement we set $\gamma = 0$ and require the magnitude of the argument of the exponential to be $\pi/4$ to effect a $\pi/2$ rotation, which maps $|\downarrow\downarrow\rangle$ to $\frac{1}{\sqrt{2}}(|\downarrow\downarrow\rangle + ie^{2i\phi} |\uparrow\uparrow\rangle)$. We simply adjust Ω to satisfy this requirement since it is a free constant parameter. If Ω is too large, we repeat the gate sequence R times to lower it by a factor of \sqrt{R} . We may also alter the axis of rotation by changing phase lag between the sidebands ϕ .

ESTIMATE OF SPIN-MOTIONAL DECOHERENCE ERROR

This section gives a simplified justification for the decoherence error estimate used in our simulation.

Suppose the internal state is an equal superposition between $|\Psi_1\rangle$ and $|\Psi_2\rangle$, which are eigenstates of some spin operator \hat{S} , with eigenvalues ± 1 . The system is subject to the effect the displacement operator $\hat{D}(\alpha) = \exp(\hat{S}(\alpha a^\dagger - \alpha^* a))$, so the two eigenstates have opposite displacements $\pm\alpha$ from the origin, which is ideally zero. Assuming that the ions are perfectly cooled to the ground state (a reasonable approximation for this experiment), the final and ideal states will be:

$$\begin{aligned} |\psi_{final}\rangle &= \frac{1}{\sqrt{2}}(|\Psi_1, \alpha\rangle + |\Psi_2, -\alpha\rangle) \\ |\psi_{ideal}\rangle &= \frac{1}{\sqrt{2}}(|\Psi_1, 0\rangle + |\Psi_2, 0\rangle) \end{aligned} \quad (10)$$

The gate fidelity is given by:

$$\begin{aligned} |\langle \psi_{final} | \psi_{ideal} \rangle|^2 &= \left| \frac{1}{2} (\langle \alpha | 0 \rangle + \langle -\alpha | 0 \rangle) \right|^2 \\ &= e^{-|\alpha|^2} \approx 1 - |\alpha|^2 \end{aligned} \quad (11)$$

Alternatively, we can trace the associated density matrix $|\psi_{final}\rangle\langle\psi_{final}|$ over the motional space. By realizing that $\text{tr}(|\alpha\rangle\langle-\alpha|) = \text{tr}(|-\alpha\rangle\langle\alpha|) = e^{-2|\alpha|^2}$, in the eigenbasis $\{|\Psi_1\rangle, |\Psi_2\rangle\}$, the final density matrix is:

$$\rho_f = \frac{1}{2} \begin{bmatrix} 1 & e^{-2|\alpha|^2} \\ e^{-2|\alpha|^2} & 1 \end{bmatrix} \quad (12)$$

And we arrive at the same fidelity:

$$F = \langle \psi_{ideal} | \rho_f | \psi_{ideal} \rangle \approx 1 - |\alpha|^2 \quad (13)$$

Since there are multiple motional modes for a multi-ion chain, the total error is simply the sum of $|\alpha|^2$ for all modes.

The motional displacement is difficult to determine since it is inherently state-dependent, and the initial state is assumed to be arbitrary. By observing the original expression for $\hat{\alpha}_k(t)$, we approximate the error as:

$$|\alpha_k| \approx \tilde{\eta} \tilde{\Omega} \left| \int_0^\tau e^{i\theta_k(t)} dt \right| \quad (14)$$

where $\tilde{\eta} = \eta_{j,0} = \Delta k \sqrt{\frac{\hbar}{2m\omega_x}} \frac{1}{\sqrt{N}}$ is the Lamb-Dicke parameter for all ions for the common mode (0.047 for 5^{171}Yb^+ ions, 0.025 for 17 ions), and $\tilde{\Omega}$ is the approximate power required to entangle a pair of qubits (about $2\pi \times 200$ kHz). Thus we define the gate error ε to be:

$$\begin{aligned} \varepsilon &\approx \sum_{k=1}^N |\alpha_k|^2 \\ &\approx (\tilde{\eta} \tilde{\Omega})^2 \sum_{k=1}^N \left| \int_0^\tau e^{i\theta_k(t)} dt \right|^2 \end{aligned} \quad (15)$$

where $\tilde{\eta}$ is the characteristic size of the Lamb-Dicke parameter, and $\tilde{\Omega}$ is the approximate power required to induce maximum entanglement between the qubit pair. Together, $\tilde{\eta} \tilde{\Omega}$ is the overall ‘‘sideband coupling strength’’, which is approximated as $2\pi \times 10$ kHz for 5 ions and $2\pi \times 5$ kHz for 17 ions.

THE ROBUSTNESS CONDITION

Since $\alpha_k \sim \int_0^\tau e^{i\theta_k(t')} dt' = 0$ is a necessary condition for guaranteeing zero displacement in the motional state space, we investigate how we can suppress α_k up to the first order in δ_1 . Replacing the phase θ_k with $\theta_k + \delta_1 t$, we evaluate the displacement through integration by parts:

$$\begin{aligned} \alpha_k(t) &\sim \int_0^\tau e^{i\theta_k(t) + i\delta_1 t} dt \approx \int_0^\tau (1 + i\delta_1 t) e^{i\theta_k(t)} dt \\ &= i\delta_1 \int_0^\tau t e^{i\theta_k(t)} dt \\ &= i\delta_1 \left(\left[t \int_0^t e^{i\theta_k(t')} dt' \right]_0^\tau - \int_0^\tau \int_0^t e^{i\theta_k(t')} dt' dt \right) \\ &= i\delta_1 (0 - \tau \alpha_{k,avg}) \end{aligned} \quad (16)$$

where $\alpha_{k,avg}$ is the time-averaged position of the trajectory from $t = 0$ to $t = \tau$. Therefore, we need it to lie on the starting point in order for α_k to remain zero up to the first order of the drift or uncertainty. Note that the approximation $e^{i\theta_k(t)} \approx 1 + i\delta_1 t$ is valid only when $\delta_1 \ll 1/\tau$. Hence, the longer the gate time, the less robust the gate becomes.

In addition, if the pulse is time-symmetric (i.e. $\delta_k(t) = \delta_k(\tau - t)$), the center of mass lying at the origin automatically guarantees that the end point will lie there as well. Thus, the robustness condition ($\alpha_{k,avg} = 0$) is a sufficient condition for displacement minimization ($\alpha_k = 0$) as long as we are restricted to symmetric pulses. The optimization criterion is now simply:

$$\alpha_{k,avg} \sim \int_0^\tau \int_0^t e^{i\theta_k(t')} dt' dt = 0, \quad k = 1, \dots, N \quad (17)$$

We seek to vary the detuning during that gate such that the above condition is satisfied. Given sufficient degrees of freedom and a good initial guess, we can arrive at an optimal pulse deterministically.

OPTIMIZATION PROCESS

Modifying the frequency allows us to alter the trajectories’ curvature, and hence their end points and time-averaged positions. In our optimization, we choose the vertices of the frequency oscillations to be our control parameters (Fig. 1). The number of vertices correspond to the degrees of freedom needed to achieve an optimal solution. It increases linearly with the number of motional modes. We connect these vertices using the cosine function to create a smoothly varying frequency pattern. This may be a useful feature, since it is difficult to vary physical parameters discretely in real experiments. The overall change in frequency (~ 100 kHz) is small compared to the frequencies used by conventional optical modulators (~ 100 MHz), minimizing sudden physical changes.

The average frequency lies above all motional modes (blue detuned), but the frequency crosses several sidebands and becomes red detuned with respect to them. The phonon number does not increase dramatically since

the driving frequency only overlaps with the sidebands momentarily.

To search for a robust frequency pattern, we define the cost function as the sum of distance squared between the center of mass of each trajectory and its starting point:

$$\begin{aligned} \text{Error} &= \sum_{k=1}^N \left| \int_0^\tau \int_0^t e^{i\theta_k(t')} dt' dt \right|^2 \\ &= \sum_{k=1}^N \left(\int_0^\tau \int_0^t \cos \theta_k(t') dt' dt \right)^2 \\ &\quad + \left(\int_0^\tau \int_0^t \sin \theta_k(t') dt' dt \right)^2 \end{aligned} \quad (18)$$

Similarly, we can define the error for a non-robust pattern as the distance squared between the trajectory end points and starting points.

It is worth noting that the optimization algorithm is inherently deterministic and requires little computational resources. For 5 sidebands, given a good initial guess, we can arrive at an optimal FM pattern in about 30 seconds using a regular laptop computer.

AREA ENCLOSED BY THE TRAJECTORY

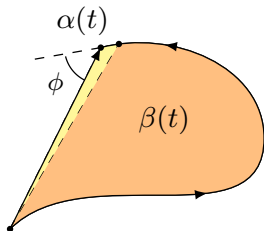


FIG. 6. An arbitrary trajectory in complex space

This section shows that the area enclosed by a trajectory has a simple expression as a double integral. Consider the following integral:

$$\alpha(t) = \int_0^t e^{i\theta(t')} dt', \quad \theta(t) = \int_0^t \delta(t') dt', \quad (19)$$

which is a general representation of a trajectory in the complex plane (see Fig. 6). At any given time t it moves at angular rate $\delta(t)$, angle $\theta(t)$, and speed 1. The area enclosed from t to $t + \delta t$ (yellow triangle in figure) is given by:

$$\begin{aligned} &\frac{1}{2} |\alpha(t)| dt \sin(\phi) \\ &= \frac{1}{2} dt \text{Im} (e^{i\theta(t)} \alpha^*(t)) \\ &= \frac{1}{2} dt \text{Im} \left(\int_0^t e^{i\theta(t) - i\theta(t')} dt' \right) \\ &= \frac{1}{2} dt \int_0^t \sin(\theta(t) - \theta(t')) dt' \end{aligned} \quad (20)$$

Hence the total area enclosed by the trajectory over a period of time t is given by:

$$\beta(t) = \frac{1}{2} \int_0^t \int_0^{t'} \sin(\theta(t') - \theta(t'')) dt'' dt', \quad (21)$$

This double integral coincides with the entanglement between two qubits after the MS gate, or rather the angle of rotation between $|\downarrow\downarrow\rangle$ and $|\uparrow\uparrow\rangle$. Hence we may evaluate how much entanglement is generated by the MS gate by observing the sizes and shapes of the PSTs.